BIOCHEMISTRY
including biophysical chemistry & molecular biology

Article

pubs.acs.org/biochemistry

Computational Insights on Crystal Structures of the Oxygen-Evolving Complex of Photosystem II with Either Ca^{2+} or Ca^{2+} Substituted by Sr^{2+}

Leslie Vogt,*[,†] Mehmed Z. Ertem,[†,‡] Rhitankar Pal,[†] Gary W. Brudvig,[†] and Victor S. Batista*[,†]

[†]Department of Chemistry, Yale University, New Haven, Connecticut 06511, United States

[‡]Chemistry Department, Brookhaven National Laboratory, Upton, New York 11973, United States

Supporting Information

ABSTRACT: The oxygen-evolving complex of photosystem II can function with either Ca^{2+} or Sr^{2+} as the heterocation, but the reason for different turnover rates remains unresolved despite reported X-ray crystal structures for both forms. Using quantum mechanics/molecular mechanics (QM/MM) calculations, we optimize structures with each cation in both the resting state (S_1) and in a series of reduced states (S_0, S_{-1}, and S_{-2}). Through comparison with experimental data, we determine that the X-ray crystal structures with either Ca^{2+} or Sr^{2+} are most consistent with the S_{-2} state (i.e., Mn_4[III,III,III,II] with O4 and O5 protonated). As expected, the QM/MM models show that Ca^{2+}/Sr^{2+} substitution results in the elongation of the heterocation bonds and the displacement of terminal waters W3 and W4. The optimized structures also show that hydrogen-bonded W5 is displaced in all S states with Sr^{2+} as the heterocation, suggesting that this water may play a critical role during water oxidation.

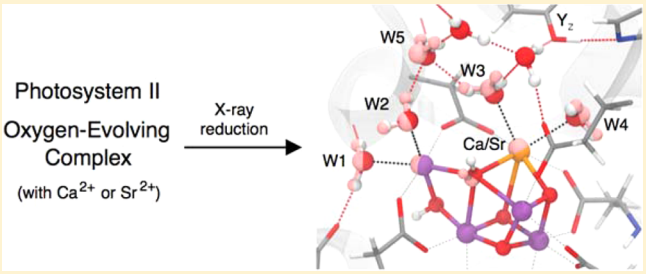

Photosystem II (PSII) is a large multisubunit protein complex found in the thylakoid membranes of higher plants and algae as well as in the internal membranes of cyanobacteria.[1−3] Using the solar energy absorbed by the reaction center chlorophylls, PSII oxidizes two water molecules and generates molecular oxygen (O_2) as a byproduct. Water oxidation occurs at the oxygen-evolving complex (OEC), which is composed of a $CaMn_4O_5$ catalytic core.[4] The catalytic mechanism requires four sequential oxidation and deprotonation steps to advance the OEC through the series of S states, of which S_0 and S_4 are the most reduced and most oxidized states, respectively.[5,6] Intriguingly, Sr^{2+} is the only cation that can functionally replace Ca^{2+} in the OEC, although it results in slower turnover rates.[7−10] In this article, we address the structural changes that might modify the function of the OEC upon substitution of Ca^{2+} by Sr^{2+}.

The X-ray diffraction (XRD) structure of PSII from a thermophilic cyanobacteria, reported at a 1.9 Å resolution (referred to herein as the Ca^{2+}-OEC, Protein Data Bank (PDB): 3ARC),[11] shows that the OEC core is a cuboidal $CaMn_3$ cluster with a dangling Mn (i.e., Mn4) and is held together by μ-oxo bridges (O1−O5) and protein side chains (Figure 1). Mn4 is linked to the cube by two μ-oxo bridges (O4 and O5), and the carboxylate group of D170 bridges it to Ca^{2+}. Two terminal water molecules (W1 and W2) bind to Mn4, and two terminal water molecules (W3 and W4) bind to Ca^{2+}. A 2.1 Å resolution XRD model of the OEC with Ca^{2+} substituted by Sr^{2+} has also been reported with a similar cuboidal OEC structure (referred to herein as the Sr^{2+}-OEC, PDB: 4IL6).[12]

In S_1, the dark-adapted resting state, the oxidation state of the OEC is most likely Mn_4[III,IV,IV,III].[13,14] (Throughout this article, square brackets are used to indicate the oxidation state of each Mn in the order reported in the 1.9 Å XRD structure.) However, during crystallographic data collection, at least 20% of the Mn centers are fully reduced to Mn(II),[3] on the basis of the X-ray-dose-dependent presence of Mn(II) in PSII samples.[15] From this, we infer that each photoreduced OEC should contain at most one Mn(II) center. In fact, it has been proposed that the 1.9 Å structure of the Ca^{2+}-OEC is reduced beyond the S_0 state,[14] possibly by one[16] or more[17,18] electrons. However, a comparison of the photoreduced structures of the Ca^{2+}-OEC and the Sr^{2+}-OEC has not yet been reported.

Building upon our previous work that was based on density functional theory quantum mechanics/molecular mechanics (DFT-QM/MM) models, calculations of extended X-ray absorption fine structure (EXAFS) spectra, and direct comparisons to experimental raw data (in k-space) for the S_1[14] and S_0[19] states of the Ca^{2+}-OEC, we now explore the effects of Sr^{2+} substitution and X-ray reduction. We report models of the OEC structure obtained at the DFT-QM/MM level in the S_1, S_0, S_{-1}, and S_{-2} states with either Ca^{2+} or Sr^{2+} as the heterocation. These models are larger than those presented

Received: September 17, 2014
Revised: December 20, 2014
Published: January 2, 2015

DOI: 10.1021/bi5011706
Biochemistry 2015, 54, 820−825

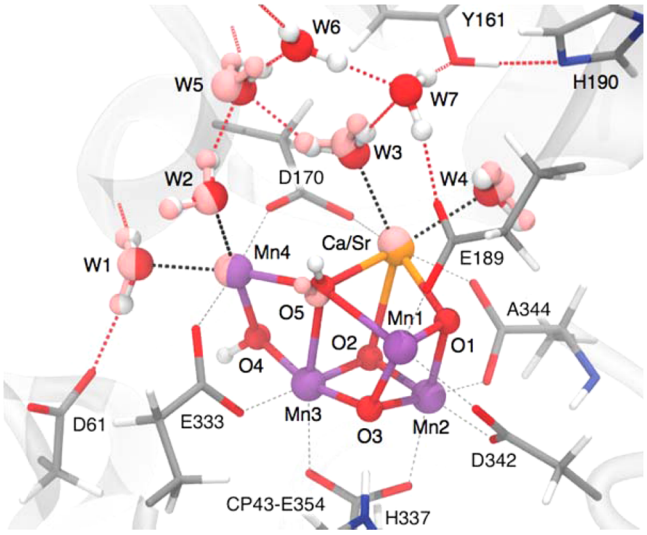

Figure 1. QM/MM-optimized structure of the Ca^{2+}-OEC in the S_{-2} state with both O4 and O5 protonated. Atoms in light red show atoms whose positions are different when Sr^{2+} is the heterocation. Bonds to OEC ligands (from subunit D1 unless otherwise noted) and terminal waters (W1–W4) are shown as gray and black dashed lines, respectively. Hydrogen bonds are shown as red dashed lines. For clarity, His332, CP43-Arg357, and other waters are not shown.

in recent work that concerned the protonation of the S_1 state,[20] and they do not consider the geometry of the OEC in the higher S states[21,22] that are not relevant in the context of the crystal structures. Comparison of our models to XRD coordinates shows that both the XRD structures of the Ca^{2+}-OEC and the Sr^{2+}-OEC best fit the S_{-2} Mn_4[III,III,III,II] state that has at least one protonated μ-oxo bridge. Furthermore, a comparison of the atomic locations between the Ca^{2+}-OEC and the Sr^{2+}-OEC in each S state reveals that the W5 water molecule bridging W2 and W3 is consistently displaced upon Sr^{2+} substitution.

COMPUTATIONAL METHODS

The DFT-QM/MM models were built and optimized using a two-layer "our own *n*-layered integrated molecular orbital and molecular mechanics" (ONIOM) H-atom-link approach[23] that was implemented in Gaussian 09 (version C.01 or D.01),[24] as recently reported for the S_0 state.[19] The QM layer includes the side chains of D1 (D61, D170, E189, H332, E333, H337, D342, and A344) and CP43 (E354 and R357) as well as ten surrounding water molecules, including those bound to Mn4 and Ca^{2+} or Sr^{2+}. We used the B3LYP functional[25,26] with the LANL2DZ pseudopotential[27,28] for Ca, Sr, and Mn and the 6-31G* basis set[29] for all other atoms. Residues with Cα atoms within 15 Å of the OEC are included in the MM layer and are described using the AMBER force field.[30] In the present work, D1-His337 is assumed to be doubly protonated; although structures with neutral D1-His337 give very similar results, the agreement with the XRD coordinates is slightly better when this residue is positively charged (Supporting Information, Section S6). The Sr^{2+}-OEC structures are prepared analogously to those of the Ca^{2+}-OEC, with Ca^{2+} substituted by Sr^{2+}. Further details of the QM/MM method can be found in the Supporting Information, along with optimized coordinates, Mn spin densities, interatomic distances for each state, and calculations of the EXAFS spectra. Thermal fluctuations are included in our EXAFS calculations as Debye–Waller factors, accounting for fluctuations of distances due to structural and/or thermal disorder under the assumption of small displacements and Gaussian distributions of distances. Although the analysis is focused on direct comparisons with experimental data at low temperature (100 K), explicit treatment of thermal fluctuations could also be modeled at room temperature by molecular dynamics simulations as previously reported.[31] Nevertheless, the reported comparison of structures at low temperature is biologically meaningful because it has been shown that temperature effects are negligible when analyzing the structure or the protonation state of PSII intermediates at 20 K and room temperature.[32]

The S_1 state is optimized with neutral terminal waters, and all μ-oxo bridges are deprotonated. Upon reduction, a proton is typically added along with each electron to maintain the net charge during oxidation-state transitions. For the S_0 state, results are reported for calculations in which the proton is placed on either O4 or O5. For the S_{-1} and S_{-2} states, both O4 and O5 are protonated.

RESULTS AND DISCUSSION

The QM/MM optimized structures show good agreement with the Mn[32] and Sr[33] K-edge EXAFS data for the S_1 state with Ca^{2+} and Sr^{2+}, respectively (Supporting Information, Section S5). Furthermore, the QM/MM models of the Ca^{2+}-OEC in the S_{-1} and S_{-2} states, each with one Mn(II), produce Mn EXAFS spectra that are similar to the spectrum of an X-ray exposed PSII-solution sample with ~25% Mn(II) content[15] (Figure S5). Although neither S_{-1} nor S_{-2} gives a complete match, the experimental data come from a fully hydrated sample that is likely to contain a mixture of states from exposure to higher X-ray doses than in the crystal structure. In general, the ability of QM/MM models to produce EXAFS spectra similar to the experimental results in several S states and with both Ca^{2+} and Sr^{2+} provides validation of our computational method.

Using the QM/MM models, we first looked for trends that result from Ca^{2+}/Sr^{2+} substitution in the OEC. Figure 1 shows the DFT-QM/MM optimized structures for the OEC in the S_{-2} state and includes the terminal water molecules bound to Ca^{2+} (red) and Sr^{2+} (light red) (analogous OEC models for the other S states are shown in Figure S3). We find that there are no long-range effects induced by Sr^{2+} on the structure of the surrounding protein. As in the Ca^{2+} and Sr^{2+} XRD structures, where the root-mean-square deviation (RMSD) of all Cα atoms for residues in the QM/MM selection is 0.09 Å,[12] the optimized QM/MM models also show good agreement in protein positions for each state. Furthermore, heterocation substitution does not significantly affect the cuboidal structure of the OEC (for an example, see the Mn–Mn distances in Tables S3 and S4). This is consistent with experimental and computational reports suggesting that the OEC structure does not undergo significant changes upon Ca^{2+} depletion[34,35] or Ca^{2+}/Sr^{2+} substitution.[36] Therefore, the heterocation is not expected to play a dominant role in the stabilization of the OEC core, which is consistent with the low occupancy of Sr^{2+} (70%) in the XRD structure.[12]

The QM/MM models indicate that Sr^{2+} is positioned slightly further away from the OEC relative to the position of Ca^{2+}, which is consistent with the larger ionic radius of Sr^{2+} versus that of Ca^{2+}. The coordination bond lengths for W3 and W4 to the heterocation are also longer for Sr^{2+} (Table 1). Another

DOI: 10.1021/bi5011706
Biochemistry 2015, 54, 820–825

change that occurs upon Ca^{2+}/Sr^{2+} substitution is in the location of the water molecule (W5) that bridges W2 and W3 via hydrogen bonds (Figure 1).

Table 1. Bond Lengths between Ca^{2+}or Sr^{2+} and μ-oxo Bridges or Terminal Waters in XRD and QM/MM Models[a]

Ca^{2+}/Sr^{2+} to:		O1	O2	O5	W3	W4
Ca^{2+} XRD[b]	A	2.33	2.49	2.49	2.39	2.49
	B	2.40	2.46	2.79	2.41	2.38
QM/MM	S_1	2.47	2.49	2.60	2.42	2.52
	S_0^{O4H}	2.45	2.87	2.46	2.45	2.53
	S_0^{O5H}	2.42	2.78	2.47	2.48	2.51
	S_{-1}	2.46	2.79	2.47	2.45	2.52
	S_{-2}	2.39	2.68	2.46	2.50	2.53
Sr^{2+} XRD[b]	A	2.42	2.64	2.56	2.54	2.32
	B	2.46	2.67	2.62	2.74	2.27
QM/MM	S_1	2.57	2.86	2.70	2.57	2.70
	S_0^{O4H}	2.58	2.99	2.58	2.57	2.70
	S_0^{O5H}	2.54	2.89	2.61	2.61	2.69
	S_{-1}	2.58	2.89	2.60	2.58	2.70
	S_{-2}	2.53	2.81	2.58	2.63	2.71

[a]Bond lengths are represented in angstroms. [b]Distances taken from XRD monomers A and B of Ca^{2+} (PDB: 3ARC)[11] and Sr^{2+} (PDB: 4IL6)[12] structures.

W5 is located between the heterocation and the active Mn centers, Mn1 and Mn4. As a hydrogen-bonded link between W2 and W3, the position of W5 directly affects the hydrogen-bonding network and the electrostatic interactions around the OEC. The altered location of W5 upon Ca^{2+}/Sr^{2+} substitution might therefore be responsible for the 3- or 4-fold increase in the exchange rate of "slow" substrate water with bulk water when Sr^{2+} is used to reconstitute Ca^{2+}-depleted PSII[37] and for the reported differences in 2D hyperfine sublevel correlation (HYSCORE) spectra.[38,39] The new positions of W3 and W5 in Sr^{2+}-substituted PSII also affect the hydrogen-bond network that connects the OEC to Y_Z (reviewed in ref 40), which may account for the slower reduction of $Y_Z^{\cdot}$ in all S states,[41] and especially in S_3.[42]

The observed shift in the W3 position is also consistent with a recent DFT model of the Sr^{2+}-OEC structure, optimized in the Mn_4[III,III,III,III] state,[43] although our DFT-QM/MM analysis suggests that the OEC S_{-1} state is Mn_4[III,IV,III,II] (Tables S1 and S2). The Mn oxidation states assigned by DFT-QM/MM are also in agreement with density matrix renormalization group (DMRG) results for S_{-1} using the Ca^{2+}-OEC XRD coordinates. However, the geometry of the OEC could not be optimized at the DMRG level, and the S_{-2} state with Mn[III,III,III,II] was not considered.[16]

The position of W4 as a terminal ligand to the heterocation is also affected by Ca^{2+}/Sr^{2+} substitution (Table 1). We note that the QM/MM structures have W4 bound to Sr^{2+} as H_2O, although the Sr−W4 bond is 0.4 Å longer than that in the XRD model. Nevertheless, the Sr K-edge EXAFS spectrum shows reasonable agreement with the experimental data (Figure S4c). We argue that the XRD position of W4 is due to a combination of the partial (only 70%) occupancy of Sr^{2+} and the crystal dehydration that can remove the hydrogen bond acceptor for W4 (i.e., the neighboring water is not resolved in monomer B),[12] although deprotonation of W4 has also been suggested as a cause.[43]

In addition to the analysis of bond lengths (Table 1), we compare the overall structure of the OEC in both the XRD and QM/MM models. We find S states with the minimum RMSDs of the OEC atoms, which were computed after aligning the QM/MM models to both of the XRD monomers with respect to the protein Cα atoms. The resulting RMSDs are shown in Figure 2 (Table S7). We find that the structures of the

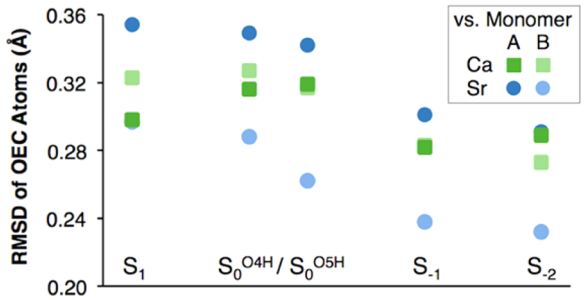

Figure 2. RMSDs for OEC atoms in the QM/MM models relative to their XRD coordinates when aligned using protein backbone atoms.

QM/MM model for the S_0 state with O5H exhibit smaller RMSDs than the analogous model with O4H, which is in accordance with our previous work that was based on the analysis of the Mn EXAFS data.[19] However, the S_{-1} and S_{-2} states with both O4 and O5 protonated fit the XRD model better than the S_1 or S_0 states with either O4H or O5H. Therefore, we propose that the OEC that is initially in the S_1 state might be quickly reduced by the X-ray radiation more than once, as it is in the presence of chemical reductants,[44] leaving a small population in the S_0 form.

An optimized linear combination of QM/MM coordinates indicates that at least 40% of both the Ca^{2+} and Sr^{2+} XRD structures are in the S_{-2} state (Supporting Information, Section S6). For the better-resolved Ca^{2+}-OEC structure, the S_1 state also contributes around 40%, which is consistent with the dark-adapted crystals being photoreduced during data collection. We note that the reduced states considered herein contain at most one Mn(II) center, unlike the more reduced state that was previously suggested as accounting for the crystal structure of the Ca^{2+}-OEC.[17,18]

For comparison, we also aligned the models that are based on the five OEC atoms with the lowest B factors: O1, Mn1, Mn2, O3, and Mn3 (see Figure S8 for XRD B factors). The subsequent RMSDs for these atoms (in all cases < 0.14 Å) are close to the experimental error and show no major change upon reduction of the OEC. Figure 3 shows the RMSDs for atoms used in the alignment (open symbols) as well as the RMSDs for the remaining OEC atoms (Ca^{2+}/Sr^{2+}, O2, O4, Mn4, and O5; shaded symbols). The second set of atoms includes those with larger B factors that are more likely to move after reduction upon X-ray radiation. For these atoms, the RMSDs are consistently larger for all S states, but unlike the protein-aligned comparison, there is no clear improvement in XRD alignment as the OEC is reduced, indicating that no one state fits all of the XRD-assigned coordinates.

To resolve which atoms are responsible for the improved structural alignment to the XRD coordinates as the OEC is reduced, we also determine the individual displacements of each atom. For the set of well-resolved OEC atoms, we again find little variation in their positions relative to their XRD coordinates for either the Ca^{2+}-OEC or the Sr^{2+}-OEC

DOI: 10.1021/bi5011706
Biochemistry 2015, 54, 820−825

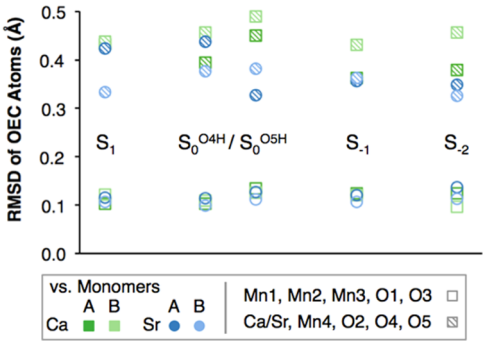

Figure 3. RMSDs for OEC atoms in the QM/MM models relative to their XRD coordinates when aligned using well-resolved OEC atoms (O1, Mn1, Mn2, O3, Mn3).

(Supporting Information, Section S6). Only in the case of O1 in monomer A of the Sr^{2+}-OEC structure is the displacement for all S states larger than the experimental error, coinciding with O1 having a larger relative B factor in this structure than in any other structure. The QM/MM position of O1 matches well with that in monomer B; this result suggests that localized QM/MM optimization is an effective tool to refine XRD-assigned coordinate positions.

For the five OEC atoms with larger B factors (Ca^{2+}/Sr^{2+}, O2, O4, Mn4, and O5), analyzing individual displacements after partial OEC alignment is instructive (Figure 4). For example, the positions of Ca^{2+} and Sr^{2+} in the S_1 QM/MM models are in line with those in the XRD data. For more reduced states, Ca^{2+} is typically closer to the Sr^{2+} XRD position (Figure 4, open symbols). In general, however, no particular trend is apparent in the displacements of Ca^{2+}/Sr^{2+} or O2 as the OEC is reduced. The larger B factors of these atoms are likely due to difficulty in resolving the electron density next to the Mn atoms rather than to atomic movement. For O4 and Mn4, the RMSDs are not improved in the more reduced S states, which is unsurprising given their large B factors and their role as atoms that move upon two-electron reduction. However, O5 behaves quite differently. In this case, there is a clear improvement in the location of the O5 atom upon protonation that is concurrent with the reduction of the OEC in our models. Because O4 is already stabilized by a water hydrogen bond, it is likely that O5 is the μ-oxo bridge that is most accessible for protonation. Because the S_1 state that best fits the EXAFS data does not have O5 protonated[15,16] and both the Ca^{2+} and Sr^{2+} XRD structures have O5 in the same position, the protonation of O5 may occur during crystal preparation or early in the data collection procedure (probably as the OEC is reduced to the S_0 state).

CONCLUSIONS

On the basis of the comparison of the bond lengths and the atomic positions in the QM/MM models to the reported XRD coordinates for PSII, we determined the effect of X-ray reduction and protonation on the structure of the OEC. The QM/MM-optimized coordinates with an S_{-2} oxidation state of Mn_4[III,III,III,II] and both O4 and O5 protonated fit the XRD data of both Ca^{2+}- and Sr^{2+}-containing PSII better than any other S state. The QM/MM models with either heterocation reproduce the XRD position of O5 only when this atom is protonated. On the basis of the optimized coordinates, we can also suggest improved positions for atoms that are difficult to resolve, such as the μ-oxo bridges that are next to the partially occupied Sr^{2+} atom. In addition, the displacement of W5 as a result of Sr^{2+} substitution in all of the S states studied herein leads us to propose that this water may play an important role in the mechanism of water oxidation.

ASSOCIATED CONTENT

Supporting Information

QM/MM method details; optimized coordinates, Mn spin densities, interatomic distances for OEC atoms, and structures for each S state; EXAFS simulations; RMSDs after protein or OEC alignment. This material is available free of charge via the Internet at http://pubs.acs.org.

AUTHOR INFORMATION

Corresponding Authors

*E-mail: leslie.vogt@gmail.com.
*E-mail: victor.batista@yale.edu. Phone: (203) 432-6672.

Present Address

L.V.: Department of Chemistry, New York University, New York, New York 10003, United States.

Funding

The authors acknowledge funding from the Division of Chemical Sciences, Geosciences, and Biosciences, Office of Basic Energy Sciences, U.S. Department of Energy grant DE-SC0001423 (V.S.B.); contract DE-AC02-98CH10886, a Computational Materials and Chemical Sciences project at Brookhaven National Laboratory (M.Z.E.); and grant DE-FG02-05ER15646 (G.W.B.).

Notes

The authors declare no competing financial interest.

ACKNOWLEDGMENTS

We thank Sahr Khan and Drs. Christian Negre, David Vinyard, and Ravi Pokhrel for helpful discussions. Figures in this manuscript were prepared with VMD[45], using colors selected

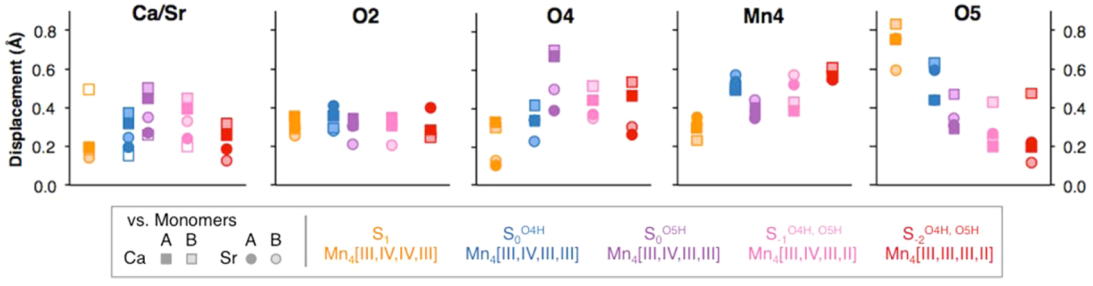

Figure 4. Displacement of selected OEC atoms for each QM/MM model relative to their X-ray coordinates when aligned using well-resolved OEC atoms.

DOI: 10.1021/bi5011706
Biochemistry 2015, 54, 820–825

from ColorBrewer 2.0.[46] We are also grateful for computer time from the High Performance Computing facilities at Yale University.

■ ABBREVIATIONS

DFT, density functional theory; DMRG, density matrix renormalization group; EXAFS, extended X-ray absorption fine structure; HYSCORE, 2D hyperfine sublevel correlation; OEC, oxygen-evolving complex; ONIOM, our own *n*-layered integrated molecular orbital and molecular mechanics; PDB, Protein Data Bank; PSII, photosystem II; QM/MM, quantum mechanics/molecular mechanics; RMSD, root-mean-square deviation; VMD, visual molecular dynamics; XRD, X-ray diffraction

■ REFERENCES

(1) Renger, G., and Renger, T. (2008) Photosystem II: The machinery of photosynthetic water splitting. *Photosynth. Res. 98*, 53−80.

(2) Dau, H., Zaharieva, I., and Haumann, M. (2012) Recent developments in research on water oxidation by photosystem II. *Curr. Opin. Chem. Biol. 16*, 3−10.

(3) Vinyard, D. J., Ananyev, G. M., and Dismukes, G. C. (2013) Photosystem II: the reaction center of oxygenic photosynthesis. *Annu. Rev. Biochem. 82*, 577−606.

(4) McEvoy, J. P., and Brudvig, G. W. (2006) Water-splitting chemistry of photosystem II. *Chem. Rev. 106*, 4455−4483.

(5) Kok, B., Forbush, B., and McGloin, M. (1970) Cooperation of charges in photosynthetic O_2 evolution. *Photochem. Photobiol. 11*, 457−475.

(6) Klauss, A., Haumann, M., and Dau, H. (2012) Alternating electron and proton transfer steps in photosynthetic water oxidation. *Proc. Natl. Acad. Sci. U.S.A. 109*, 16035−16040.

(7) Ghanotakis, D. F., Babcock, G. T., and Yocum, C. F. (1984) Calcium reconstitutes high rates of oxygen evolution in polypeptide depleted photosystem II preparations. *FEBS Lett. 167*, 127−130.

(8) Boussac, A., and Rutherford, A. W. (1988) S-state Formation after Ca^{2+} depletion in the Photosystem II Oxygen-Evolving Complex. *Chem. Scr. 28A*, 123−126.

(9) Vrettos, J. S., Stone, D. A., and Brudvig, G. W. (2001) Quantifying the ion selectivity of the Ca^{2+} site in photosystem II: Evidence for direct involvement of Ca^{2+} in O_2 formation. *Biochemistry 40*, 7937−7945.

(10) Boussac, A., Rappaport, F., Carrier, P., Verbavatz, J.-M., Gobin, R., Kirilovsky, D., Rutherford, A. W., and Sugiura, M. (2004) Biosynthetic Ca^{2+}/Sr^{2+} exchange in the photosystem II oxygen-evolving enzyme of *Thermosynechococcus elongatus*. *J. Biol. Chem. 279*, 22809−22819.

(11) Umena, Y., Kawakami, K., Shen, J.-R., and Kamiya, N. (2011) Crystal structure of oxygen-evolving photosystem II at a resolution of 1.9 Å. *Nature 473*, 55−60.

(12) Koua, F. H. M., Umena, Y., Kawakami, K., and Shen, J.-R. (2013) Structure of Sr-substituted photosystem II at 2.1 Å resolution and its implications in the mechanism of water oxidation. *Proc. Natl. Acad. Sci. U.S.A. 110*, 3889−3894.

(13) Kulik, L. V., Epel, B., Lubitz, W., and Messinger, J. (2007) Electronic structure of the Mn_4O_xCa cluster in the S_0 and S_2 states of the oxygen-evolving complex of photosystem II based on pulse ^{55}Mn-ENDOR and EPR spectroscopy. *J. Am. Chem. Soc. 129*, 13421−13435.

(14) Luber, S., Rivalta, I., Umena, Y., Kawakami, K., Shen, J.-R., Kamiya, N., Brudvig, G. W., and Batista, V. S. (2011) S_1-state model of the O_2-evolving complex of photosystem II. *Biochemistry 50*, 6308−6311.

(15) Yano, J., Kern, J., Irrgang, K.-D., Latimer, M. J., Bergmann, U., Glatzel, P., Pushkar, Y., Biesiadka, J., Loll, B., and Sauer, K. (2005) X-ray damage to the Mn_4Ca complex in single crystals of photosystem II: a case study for metalloprotein crystallography. *Proc. Natl. Acad. Sci. U.S.A. 102*, 12047−12052.

(16) Kurashige, Y., Chan, G. K.-L., and Yanai, T. (2013) Entangled quantum electronic wavefunctions of the Mn_4CaO_5 cluster in photosystem II. *Nat. Chem. 5*, 660−666.

(17) Galstyan, A., Robertazzi, A., and Knapp, E. W. (2012) Oxygen-evolving Mn cluster in photosystem II: The protonation pattern and oxidation state in the high-resolution crystal structure. *J. Am. Chem. Soc. 134*, 7442−7449.

(18) Grundmeier, A., and Dau, H. (2012) Structural models of the manganese complex of photosystem II and mechanistic implications. *Biochim. Biophys. Acta, Bioenerg. 1817*, 88−105.

(19) Pal, R., Negre, C. F. A., Vogt, L., Pokhrel, R., Ertem, M. Z., Brudvig, G. W., and Batista, V. S. (2013) S_0-State Model of the Oxygen-Evolving Complex of Photosystem II. *Biochemistry 52*, 7703−7706.

(20) Robertazzi, A., Galstyan, A., and Knapp, E. W. (2014) PSII manganese cluster: protonation of W2, O5, O4 and His337 in the S_1 state explored by combined quantum chemical and electrostatic energy computations. *Biochim. Biophys. Acta, Bioenerg. 1837*, 1316−1321.

(21) Pantazis, D. A., Ames, W., Cox, N., Lubitz, W., and Neese, F. (2012) Two interconvertible structures that explain the spectroscopic properties of the oxygen-evolving complex of photosystem II in the S_2 state. *Angew. Chem., Int. Ed. 51*, 9935−9940.

(22) Cox, N., Retegan, M., Neese, F., Pantazis, D. A., Boussac, A., and Lubitz, W. (2014) Electronic structure of the oxygen-evolving complex in photosystem II prior to O-O bond formation. *Science 345*, 804−808.

(23) Vreven, T., Morokuma, K., Farkas, O., Schlegel, H. B., and Frisch, M. J. (2003) Geometry optimization with QM/MM, ONIOM, and other combined methods. I. Microiterations and constraints. *J. Comput. Chem. 24*, 760−769.

(24) Frisch, M. J., Trucks, G. W., Schlegel, H. B., Scuseria, G. E., Robb, M. A., Cheeseman, J. R., Scalmani, G., Barone, V., Mennucci, B., Petersson, G. A., Nakatsuji, H., Caricato, M., Li, X., Hratchian, H. P., Izmaylov, A. F., Bloino, J., Zheng, G., Sonnenberg, J. L., Hada, M., Ehara, M., Toyota, K., Fukuda, R., Hasegawa, J., Ishida, M., Nakajima, T., Honda, Y., Kitao, O., Nakai, H., Vreven, T., Montgomery, J. A., Jr., Peralta, J. E., Ogliaro, F., Bearpark, M., Heyd, J. J., Brothers, E., Kudin, K. N., Staroverov, V. N., Kobayashi, R., Normand, J., Raghavachari, K., Rendell, A., Burant, J. C., Iyengar, S. S., Tomasi, J., Cossi, M., Rega, N., Millam, J. M., Klene, M., Knox, J. E., Cross, J. B., Bakken, V., Adamo, C., Jaramillo, J., Gomperts, R., Stratmann, R. E., Yazyev, O., Austin, A. J., Cammi, R., Pomelli, C., Ochterski, J. W., Martin, R. L., Morokuma, K., Zakrzewski, V. G., Voth, G. A., Salvador, P., Dannenberg, J. J., Dapprich, S., Daniels, A. D., Farkas, Ö., Foresman, J. B., Ortiz, J. V., Cioslowski, J., and Fox, D. J. (2009) *Gaussian 09*, version D.01, Gaussian, Inc., Wallingford, CT.

(25) Becke, A. D. (1993) Density-functional thermochemistry. III. The role of exact exchange. *J. Chem. Phys. 98*, 5648−5652.

(26) Lee, C., Yang, W., and Parr, R. G. (1988) Development of the Colle-Salvetti correlation-energy formula into a functional of the electron density. *Phys. Rev. B 37*, 785−789.

(27) Hay, P. J., and Wadt, W. R. (1985) Ab initio effective core potentials for molecular calculations. Potentials for the transition metal atoms Sc to Hg. *J. Chem. Phys. 82*, 270−283.

(28) Wadt, W. R., and Hay, P. J. (1985) Ab initio effective core potentials for molecular calculations - Potentials for main group elements Na to Bi. *J. Chem. Phys. 82*, 284−298.

(29) Hariharan, P. C., and Pople, J. A. (1973) The influence of polarization functions on molecular orbital hydrogenation energies. *Theor. Chim. Acta 28*, 213−222.

(30) Case, D. A., Darden, T. A., Cheatham, T. E. I., Simmerling, C. L., Wang, J., Duke, R. E., Luo, R., Walker, R. C., Zhang, W., Merz, K. M., Roberts, B., Hayik, S.Roitberg, A., Seabra, G., Swails, J., Goetz, A. W., Kolossváry, I., Wong, K. F., Paesani, F., Vanicek, J., Wolf, R. M., Liu, J., Wu, X., Brozell, S. R., Steinbrecher, T., Gohlke, H., Cai, Q., Ye, X., Wang, J., Hsieh, M. J., Cui, G., Roe, D. R., Mathews, D. H., Seetin, M. G., Salomon-Ferrer, R., Sagui, C., Babin, V., Luchko, T., Gusarov,

DOI: 10.1021/bi5011706
Biochemistry 2015, 54, 820−825

S., Kovalenko, A., Kollman, P. A. (2012) *Amber* 12, University of California, San Francisco, CA.
(31) Rivalta, I., Amin, M., Luber, S., Vassiliev, S., Pokhrel, R., Umena, Y., Kawakami, K., Shen, J. R., Kamiya, N., Bruce, D., Brudvig, G. W., Gunner, M. R., and Batista, V. S. (2011) Structural-functional role of chloride in photosystem II. *Biochemistry 50*, 6312−6315.
(32) Haumann, M., Müller, C., Liebisch, P., Iuzzolino, L., Dittmer, J., Grabolle, M., Neisius, T., Meyer-Klaucke, W., and Dau, H. (2005) Structural and oxidation state changes of the photosystem II manganese complex in four transitions of the water oxidation cycle ($S_0 \rightarrow S_1$, $S_1 \rightarrow S_2$, $S_2 \rightarrow S_3$, and $S_{3,4} \rightarrow S_0$) characterized by X-ray absorption spectroscopy at 20 K and room temperature. *Biochemistry 44*, 1894−1908.
(33) Cinco, R. M., Robblee, J. H., Rompel, A., Fernandez, C., Yachandra, V. K., Sauer, K., and Klein, M. P. (1998) Strontium EXAFS reveals the proximity of calcium to the manganese cluster of oxygen-evolving photosystem II. *J. Phys. Chem. B 102*, 8248−8256.
(34) Lohmiller, T., Cox, N., Su, J. H., Messinger, J., and Lubitz, W. (2012) The basic properties of the electronic structure of the oxygen-evolving complex of photosystem II are not perturbed by Ca^{2+} removal. *J. Biol. Chem. 287*, 24721−24733.
(35) Saito, K., and Ishikita, H. (2014) Influence of the Ca^{2+} ion on the Mn_4Ca conformation and the H-bond network arrangement in Photosystem II. *Biochim. Biophys. Acta 1837*, 159−166.
(36) Cox, N., Rapatskiy, L., Su, J. H., Pantazis, D. A., Sugiura, M., Kulik, L., Dorlet, P., Rutherford, A. W., Neese, F., Boussac, A., Lubitz, W., and Messinger, J. (2011) Effect of Ca^{2+}/Sr^{2+} substitution on the electronic structure of the oxygen-evolving complex of photosystem II: a combined multifrequency EPR, ^{55}Mn-ENDOR, and DFT study of the S_2 state. *J. Am. Chem. Soc. 133*, 3635−3648.
(37) Hendry, G., and Wydrzynski, T. (2003) ^{18}O isotope exchange measurements reveal that calcium is involved in the binding of one substrate-water molecule to the oxygen-evolving complex in photosystem II. *Biochemistry 42*, 6209−6217.
(38) Milikisiyants, S., Chatterjee, R., Coates, C. S., Koua, F. H. M., Shen, J.-R., and Lakshmi, K. V. (2012) The structure and activation of substrate water molecules in the S_2 state of photosystem II studied by hyperfine sublevel correlation spectroscopy. *Energy Environ. Sci. 5*, 7747−7756.
(39) Chatterjee, R., Milikisiyants, S., Coates, C. S., Koua, F. H., Shen, J. R., and Lakshmi, K. V. (2014) The structure and activation of substrate water molecules in Sr^{2+}-substituted photosystem II. *Phys. Chem. Chem. Phys. 16*, 20834−20843.
(40) Pokhrel, R., and Brudvig, G. W. (2014) Oxygen-Evolving Complex of Photosystem II: Correlating structure with spectroscopy. *Phys. Chem. Chem. Phys. 16*, 11812−11821.
(41) Westphal, K. L., Lydakis-Simantiris, N., Cukier, R. I., and Babcock, G. T. (2000) Effects of Sr^{2+}-substitution on the reduction rates of Yz in PSII membranes evidence for concerted hydrogen-atom transfer in oxygen evolution. *Biochemistry 39*, 16220−16229.
(42) Rappaport, F., Ishida, N., Sugiura, M., and Boussac, A. (2011) Ca^{2+} determines the entropy changes associated with the formation of transition states during water oxidation by Photosystem II. *Energy Environ. Sci. 4*, 2520−2524.
(43) Terrett, R., Petrie, S., Pace, R. J., and Stranger, R. (2014) What does the Sr-substituted 2.1 Å resolution crystal structure of photosystem II reveal about the water oxidation mechanism? *Chem. Commun. (Cambridge, U.K.) 50*, 3187−3190.
(44) Riggs, P. J., Mei, R., Yocum, C. F., and Penner-Hahn, J. E. (1992) Reduced derivatives of the manganese cluster in the photosynthetic Oxygen-Evolving Complex. *J. Am. Chem. Soc. 114*, 10650−10651.
(45) Humphrey, W., Dalke, A., and Schulten, K. (1996) VMD: Visual Molecular Dynamics. *J. Mol. Graphics 14*, 33−38.
(46) Brewer, C. A. *ColorBrewer* 2.0, http://www.colorbrewer2.org (accessed April 1, 2014).

DOI: 10.1021/bi5011706
Biochemistry 2015, 54, 820−825